Exciton dynamics in highly excited CdSe studied by picosecond gain-absorption spectroscopy

T. Amand, J. Collet, and B. S. Razbirin*

Laboratoire de Physique des Solides, Institut National des Sciences Appliquées, Université Paul Sabatier, Avenue de Rangueil, 31077 Toulouse Cedex, France

(Received 23 December 1985)

We report here on the exciton dynamics in highly excited CdSe studied by picosecond time-resolved gain-absorption spectroscopy. In particular, we study simultaneously both the spectral region of the direct processes (to get information of the bound-state stability) and the region of the LO-phonon-assisted processes (to get information on the quasiparticle temperature and density). We deduce the temperature and the density kinetics of the exciton gas just below the Mott transition. The stability of the $1S$ and $2S$ exciton states is discussed in relation to the available theoretical criteria. We conclude that in the dynamical regime excitons can be formed at densities higher than the density given by the Mott criterion. Concerning the $2S$ state, we show that it remains stable in an exciton gas, the density of which is lower than $\rho_c(n=2)=(3/4\pi)[4a_B(n=1)]^{-3}$.

I. INTRODUCTION

Dense excitonic systems in direct-gap semiconductors have been investigated during the last decade by employing several experimental techniques. The studies are focused either on optical properties, or on the electronic properties of the material. In nanosecond experiments,[1] these systems are studied in quasistationary conditions. One main feature displayed by transmission or reflectivity experiments is the disappearance of the excitonic structures when increasing the excitation power (see, e.g., Ref. 2 for GaAs, Refs. 3–5 for CdS, Refs. 5 and 6 for ZnO). In luminescence experiments, numerous radiative excitonic processes such as the inelastic exciton-exciton or exciton-free carrier collisions appear under strong excitation, besides the exciton annihilation in one polariton-photon and m-LO phonons ($m = 1,2,...$).[7–9] A biexciton can decay into one exciton and one polariton photon at such excitation regimes, as was clearly evidenced in large gap materials.[10] As all these processes give rise to amplification of the spontaneous luminescence, more quantitative results on dense excitonic systems were obtained by measuring the optical gain (see, e.g., Refs. 5, 7, 8 and 11 for CdS, and Ref. 12 for ZnO).

With the subsequent development of picosecond and subpicosecond excitation sources, it became possible to gain insight into the kinetics of electronic processes. Transient absorption (or reflectivity) studies, in the vicinity of the excitonic resonance, were performed using polychromatic subpicosecond pulse and probe experiments, in order to elucidate the screening dynamics of the electron-hole interaction in the exciton-plasma systems (see, e.g., Ref. 13 for CuCl, Ref. 14 for CdSe). The problem of screening in a dense exciton system was investigated in GaAs.[15] In all these experiments, one critical limitation originates in the difficulty of estimating precisely both the density and the temperature of the electron-hole system. On the other hand, picosecond time-resolved photoluminescence experiments enabled us to study the kinetics of excitonic processes (see, e.g., Refs. 16–19 for CdSe, Refs. 20 and 21 for CdS, Ref. 19 for CuI, and Ref. 22 for ZnO). In particular, the temperature kinetics of the excitonic system could be deduced from the decay of the exciton-LO process.[16,17,19]

In the present work, using a pulse and polychromatic probe technique, we measured simultaneously the absorption of the direct processes and the gain of the LO-phonon-assisted processes. So we obtained information both on the exciton stability and on the temperature and the density of the exciton-plasma system. We stress here that the gain measurement provides a unique tool for determining the density of a nondegenerate exciton gas, which is impossible using the luminescence technique. We used a two-photon generation of the electron-hole pairs to ensure a homogeneous creation of the electron-hole plasma within the sample. We observed the kinetics of the plasma-exciton transition in CdSe. We deduced from our experiments the kinetics of the temperature and density of excitons. The stability of the $1S$ and $2S$ exciton states at high density are discussed. We show that the $2S$ state becomes stable in an exciton gas, when the density falls below $\rho_c(n=2)(3/4\pi)[4a_B(n=1)]^{-3}$.

In Sec. II, we describe the experimental setup and the experimental conditions. In Sec. III we describe and interpret the experimental results, in Sec. IV we deduce the exciton dynamics, and conclude in Sec. V with a discussion on the stability of electron-hole bound states.

II. EXPERIMENTAL SETUP AND PROCEDURE

The experimental technique we used was the time-resolved pulse and probe transmission spectroscopy, for measuring simultaneously the excitation-induced amplification as well as the absorbing processes. The probe was polychromatic. Note that this technique is more powerful than the method of the variable excitation strip length (Refs. 7 and 8), which permits to measure the gain or the absorption of only the emission processes.
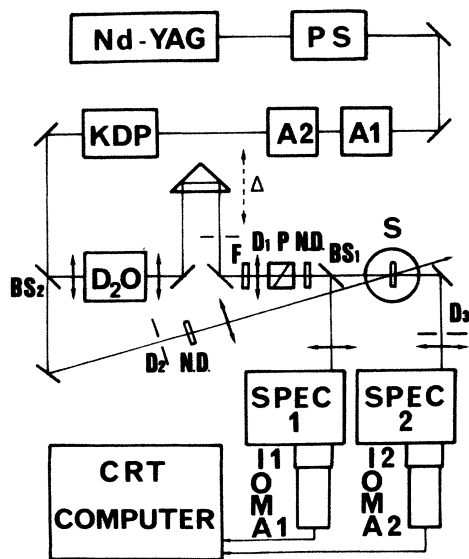
FIG. 1. Experimental setup for time-resolved transmission spectroscopy. $A_{1,2}$, YAG: ND^{3+} amplifiers; PS, pulse slicer; KDP, second harmonic generator; $BS_{1,2}$, beam splitters; $D_{1,2,3}$, diaphragms; Δ, variable optical path length; F, filter; ND, neutral density; S, sample; $SPEC_{1,2}$, spectrometers; $IOMA_{1,2}$, intensified optical multichannel analyzers; CRT, simultaneously displays the incident and transmitted probe.

FIG. 2. Sample orientation: both the crystallographic c axis and the probe polarization vector ϵ are parallel to the plane of incidence (II). $\phi_{i(t)}$: incident (transmitted) photon flux of the probe pulse; $\theta = (\epsilon, c)$; ϕ_{ex} denotes the excitation photon flux.

The experimental setup is displayed in Fig. 1. An active and passive mode-locked neodymium-doped yttrium aluminum garnet (YAG:Nd^{3+}) laser coupled with a pulse slicer delivers single infrared pulses at wavelength $\lambda_{ex} = 1064$ nm and of duration $\Delta t \simeq 30$ ps [full width at half maximum (FWHM)]. After pulse amplification, a potassium dideuterium phosphate (KD_DP) crystal converts up to 40% of the incident energy by frequency doubling, at $\lambda_1 = 532$ nm. A beam splitter (BS2) separates the green from the infrared pulse. The latter excites the sample. The green pulse is focused into a D_2O cell in order to generate a broad-band continuum. The fluctuations due to the inherent instabilities of the polychromatic pulses are greatly reduced by using a two-way detection system which records simultaneously the incident and the transmitted light (see below). The time behavior of the probe pulse was analyzed in a preliminary experiment by means of an optical sampling gate—a CS_2 Kerr shutter. We estimated the temporal width of the probe to be lower than or equal to 30 ps (FWHM), which yields the time resolution of the transmission experiment.

The sample was an as-grown CdSe platelet of thickness $d \simeq 30$ μm, immersed in liquid helium at $T_b = 4.2$ K. The electron-hole pair generation was achieved by means of two-photon absorption of the excitation pulse at 1064 nm, thus creating a quasihomogeneous carrier density throughout the platelet:[16,17] for instance, at the excitation power $\phi_{ex} \simeq 300$ MW/cm^2, using $\beta \simeq 0.03$ cm MW^{-1} and $R \simeq 0.26$, respectively, for the two-photon absorption coefficient and the reflection coefficient at the excitation wavelength, a simple estimation yields an overall 2% attenuation of the photon flux within the platelet. The po-
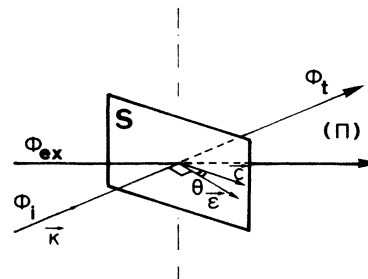
larization direction of the probe and the crystal c axis were parallel to the plane of incidence II (see Fig. 2) so that at normal incidence, the transition from the ground state to the $A_T^{1S}(\Gamma_5)$ state is dipole forbidden. Then, by slightly tilting the sample with a small angle θ around the vertical axis $(\theta \sim 5°)$ to allow a weak coupling between photons and exciton states, we could adjust the A^{1S} absorption line to be equal to the full dynamics of the transmission spectrum. This is the so-called mixed-mode configuration which was chosen in order to avoid absorption saturation through the sample, despite its thickness. A set of filters (F) cuts the frequencies above 1.85 eV in order to minimize carrier generation by the probe, which is attenuated until the A^{2S} absorption line is clearly featured by the transmitted spectra. A broad-band semitransparent mirror (BS1) reflects about 50% of the probe energy to simultaneously analyze the incident and transmitted spectra. The detection system consists of two identical channels, each one being composed of a spectrometer, a light intensifier coupled with an optical multichannel analyzer. Both ways are monitored by a computer. The excitation and probe spots were, respectively, 100 and 50 μm wide, so we analyze only the center of the excited region.

The transmission function $T(h\nu, t)$ is now obtained as follows: the incident and transmitted spectra, denoted, respectively, $\phi_{in}(h\nu)$ and $\phi_{tr}(h\nu, t)$ are cumulated over typically 10^3 shots.[23] The relative transfer function ψ_{tr}/ϕ_{in} between the two channels was previously determined by making a similar recording without sample. The transmission function (as displayed, for example, in Fig. 3) now reads

$$T(h\nu, t) = \delta \left[\frac{\phi_{tr}(h\nu, t)}{\phi_{in}(h\nu)} \right] \left[\frac{\psi_{tr}(h\nu)}{\psi_{in}(h\nu)} \right]^{-1}. \tag{1}$$

Here, δ is a proportionality constant which can be calibrated in the transparent spectral region of the unexcited sample, if necessary. The excitation-induced gain spectra in the latter region can also be obtained in a simpler way by computing the ratios (see, for instance, Fig. 4):
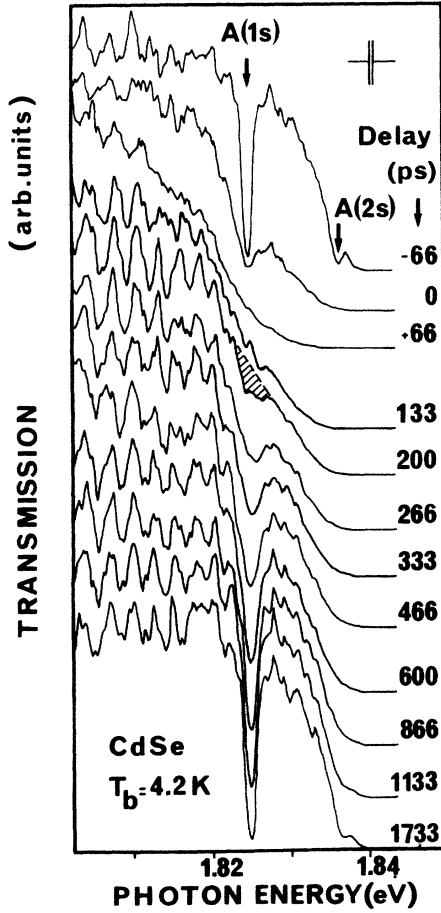
FIG. 3. Time-resolved transmission spectra of CdSe around the A^{1S} excitonic region. The A^{1S} absorption line which has disappeared after the excitation pulse (see spectrum at $t = 66$ ps) is already present, although considerably broadened, at $t = 200$ ps, as indicated by the hatched area on the corresponding spectrum. The A^{2S} absorption line is clearly seen on the unexcited sample ($t = -66$ ps) and at $t = 1.7$ ns. (The symbol on the upper right corner indicates the spectral resolution.)

FIG. 4. Excitation-induced transmission relative to the unexcited sample. (Same data as Fig. 3.) The gain ($S_\alpha > 1$) on the A-LO process, which peaks at 1.80 eV, is detected from $t = 133$ to 1733 ps. (The symbol on the upper right corner indicates the spectral resolution; the ordinate origins of the different spectra are shifted for clarity.)

$$S_\alpha(h\nu,t) = \left[\frac{\phi_{tr}(h\nu,t)}{\phi_{in}(h\nu)} \right] \left[\frac{\phi_{tr}(h\nu, -\infty)}{\phi_{in}(h\nu)} \right]^{-1} . \qquad (2)$$

Here, $\phi_{tr}(h\nu, -\infty)$ represents the transmitted signal without excitation, which is obtained practically for $t \leq -66$ ps or $t > 2$ ns. At those delays, we obtain $\tilde{S}_\alpha(h\nu,t) = 1 \pm 0.06$ on the entire analyzed spectral range, thus yielding the accuracy of the transmission measurement. The amplification coefficient $\alpha(h\nu,t)$ can then be deduced easily by solving the equation:

$$S_\alpha(h\nu,t) = \frac{e^{\alpha d}(1 - R^2)}{1 - R^2 e^{2\alpha d}} , \qquad (3)$$

since the reflection coefficient is nearly excitation independent in this region (see, e.g., Ref. 24). Equations (2) and (3) allow a rather simple determination of the excitation-induced gain in the spectral region where the crystal is transparent before the arrival of the excitation
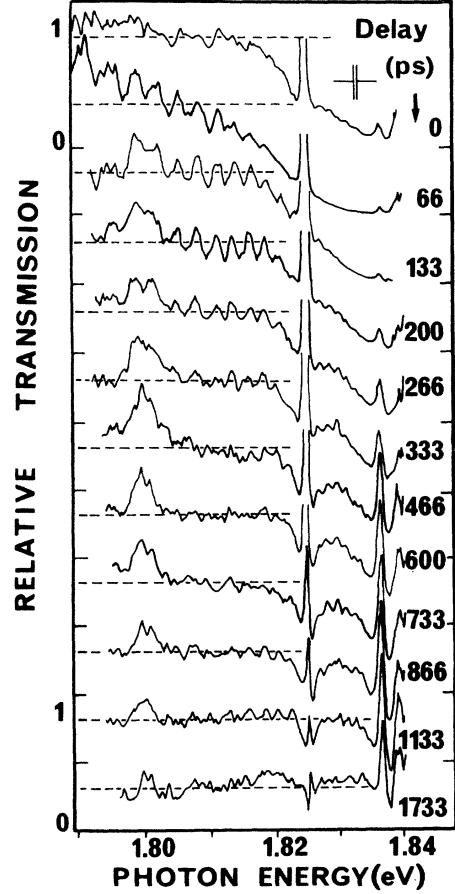
pulse, i.e., for photon energies $h\nu \lesssim 1.82$ eV. In this energy range, the inequality

$$|\alpha(h\nu,t)| \gg |\alpha(h\nu, -\infty)|$$

holds. While summing the multiple reflections within the platelet, we did not take into account the phase factors, so that expression (3) represents an average value. This approximation is justified here since the modulation depth due to Fabry-Perot interferences featured by the transmitted spectra was much smaller than the transmitted signal amplitude (see Fig. 3). We attributed the damping of these oscillations mainly to the imperfections of the sample surface.

III. EXPERIMENTAL RESULTS AND INTERPRETATION

Figure 3 displays the transient behavior of the sample transmission function (1) at different time delays with respect to the excitation pulse. The peak power amounted

to 300 MW/cm^2. The transmission spectrum without excitation is measured at $t = -66$ ps, and clearly displays the A^{1S} and A^{2S} excitonic structures. These structures thereafter completely disappear from the spectra at $t = 66$ ps, thus indicating that electron-hole bound states no longer exist. The electronic system is now in a plasma metallic state electron-hole plasma (EHP) and the peak pair density is reached at this time. The absorption is mainly governed by band-to-band transitions through a renormalized band gap. Then, when increasing the probe delay to about 200 ps, the A^{1S} excitonic resonance reappears. Now the line is much broader and the absorption weaker than in the unexcited sample, indicating a strong damping and a reduction of the transition oscillator strength. The A^{1S} absorption line gradually recovers up to 1.5 ns. No clear shift of this line could be detected within our experimental resolution. This indicates a rather exact compensation between the renormalization of electron and hole band states and the decrease of the exciton binding energy due to screening of the Coulomb interaction, as was featured by previous theoretical calculations.[25]

The transient behavior of the A^{2S} excitonic resonance could also be observed: The corresponding absorption line already disappears during the excitation pulse at $t \simeq 0$; it recovers much later than the A^{1S} structure, and is clearly observed at time $t \simeq 1.7$ ns. This is obviously due to the lower binding energy of the exciton excited state $2S$. The reproducible oscillations superimposed on the transmission spectra are due to Fabry-Perot interferences within the platelet.

Time-resolved amplification spectra are displayed in Fig. 4. They were recorded simultaneously with the data displayed in Fig. 3, but now the simpler numerical treatment (2) is applied. The different spectra are shifted vertically in the figure for clarity. The part of each spectrum above the dashed line corresponds to gain. Two processes clearly appear when the probe delay increases. First, for $0 \lesssim t < 133$ ps, a broad amplification band is present at spectral energies lower than or equal to about 1.8 eV. Then for $t \gtrsim 133$ ps, it disappears, leaving a new amplification line which peaks at 1.800 eV and dominates the transmission spectra until the delay 1.7 ns. The spectral position of the gain line corresponds exactly to the recombination process of the free exciton assisted by one LO phonon emission already observed in numerous luminescence experiments[16,17,19,26] and labeled hereafter A-LO. Moreover, the emergence of our amplification line is correlated to the appearance of the A^{1S} excitonic structure in the transmission spectra for delays $133 \lesssim t \lesssim 200$ ps. So we attribute unambiguously our line at 1.800 eV to amplification by the A-LO process. At the beginning of the kinetics, no electron-hole bound states are present, as proved by Fig. 3. So we attribute the initial broad band displayed in Fig. 4 to LO-phonon-assisted recombination of electron-hole pairs in a plasma, denoted hereafter, EHP-LO. The main features of the transient behavior of the electron-hole system are very similar to those we reported in previous time-resolved luminescence experiments performed under the same experimental conditions (see, e.g., in Ref. 16, the spectra obtained for $P_{ex} \simeq 300$ MW/cm^2):

For instance, in the plasma regime at the beginning of the kinetics, the direct processes in the spectral region ranging from 1.81 to 1.82 eV correspond to absorption, as can be seen in Fig. 4, for $t \simeq 66$ ps, while the LO-phonon-assisted processes correspond to stimulated emission. This is just what we already claimed in Ref. 20 and is clearly demonstrated in the present experiment: due to the high initial kinetic energy E_c of the generated electron-hole pairs ($E_c \simeq 490$ meV), the plasma is hot during and just after the excitation pulse, thus giving rise to absorption in the region of direct processes.

Transient oscillation structures are clearly seen for time delays ranging from $66 \lesssim t \lesssim 333$ ps, indicating an excitation-induced modification of the dielectric constant. When the electron-hole pair density increases, the index of refraction decreases, leading to a shift of the interference extrema towards shorter wavelengths,[24] according to the relation (e.g., for the maxima):

$$2n(\lambda_{max}, t)d = m\lambda_{max} .$$

Here, λ_{max} is the vacuum wavelength of the maximum of order m (integer) and n is the real part of the refractive index. Thus very small relative variations of n induce detectable shifts of those maxima.

IV. EXCITON DYNAMICS

The temperature and the density kinetics of the exciton gas can be deduced from the transient gain spectroscopy by analyzing the position and the width of the band ascribed to the A-LO process. Within a small energy range around the minimum spectral energy of the A-LO process (neglecting polariton effects), the amplification coefficient reads simply:[1,7,27]

$$\alpha_{A\text{-LO}}(h\nu) = C(h\nu - E_{ex} + \hbar\omega_{LO})^{3/2}(b_{ex} - b_{LO}) . \quad (4)$$

The notations are as follows: C, constant coefficient in the spectral range defined above (proportional to the exciton-LO phonon square of the matrix element); E_{ex}, energy of the A^{1S} exciton level; $\hbar\omega_{LO}$, phonon energy; b_{ex} and b_{LO}, respectively, the occupation functions of the exciton states and of the LO-phonons. They are defined by

$$b_{ex}(E) = \left[\exp\left[\frac{E - \mu_{ex}}{kT}\right] - 1\right]^{-1},$$

$$b_{LO} = \left[\exp\left[\frac{\hbar\omega_{LO}}{kT_L}\right] - 1\right]^{-1},$$

where μ_{ex} denotes the exciton chemical potential. T_{ex} and T_{LO} are, respectively, the exciton and lattice temperatures.

In a nondegenerate exciton system, the chemical potential μ_{ex} is related to the exciton density ρ_{ex} by the usual following formula:

$$\rho_{ex} = g_{ex}\left[\frac{2\pi M_{ex}kT_{ex}}{h^2}\right]^{3/2} \exp\left[\frac{\mu_{ex}}{kT_{ex}}\right] . \quad (5)$$

Here, T_{ex} denotes the exciton temperature; M_{ex}, the exciton translation mass; and g_{ex}, the degeneracy of the exci-

ton level. We take $g_{ex} = 4$ as we do not treat separately the different excitonic $(1S)$ bands in the temperature range investigated (see below and Fig. 6). Moreover, since the lattice is cold, for the excitonic density and temperature ranges of interest here, the condition,

$$b_{ex} \gg b_{LO} , \qquad (6)$$

holds during the whole kinetics (as can be checked self-consistently below).

From (4) and (5) and condition (6), one easily deduces that the maximum amplification of the A-LO process is obtained at the frequency:

$$h\nu_M = E_{ex} - \hbar\omega_{LO} + \tfrac{3}{2}kT_{ex} , \qquad (7)$$

and reads

$$\alpha_M = C\frac{\rho_{ex}}{g_{ex}} \left[\frac{3\pi\hbar^2}{M_{ex}} \right] \exp(-\tfrac{3}{2}) . \qquad (8)$$

Here, taking

$$M_{ex} = \left[M_{ex}^{\parallel} \left[M_{ex}^{\perp} \right]^2 \right]^{1/3} = 0.59m_0$$

(deduced from Ref. 28), we obtain the numerical expression:

$$\alpha_n = 2.37 \times 10^{-18} C\rho_{ex} \text{ cm}^{-1} , \qquad (8')$$

(C in $\text{cm}^{-1}\text{meV}^{-3/2}$ and ρ in cm^{-3}).

The amplitude of the matrix element of the A-LO process can be calibrated using previous absorption edge experiments (in the range $E_{ex} - \hbar\omega_{LO} < h\nu < E_{ex}$) at moderate temperature ($T_L \sim 77$ K) and low excitation level.[29] Here, the reverse of condition (6) is fulfilled: $b_{LO} \gg b_{ex}$. Using the exciton absorption edge theory,[30] we estimate an effective coefficient C_{eff} for the A-LO process under our experimental conditions.[31] We find

$$C_{eff} = 240 \pm 90 \text{ cm}^{-1}\text{meV}^{-3/2} ,$$

and use $C = C_{eff}$. The kinetics of α_M deduced from the data through relation (3) are displayed in Fig. 5. The corresponding density kinetics are also shown. Here we assume the exciton LO-phonon coupling is constant for the whole exciton kinetics. For $133 \leq t \leq 466$ ps, the gain line increases. This corresponds to the formation of excitons from the electron-hole pairs of the plasma. At this stage, bound and unbound pairs coexist. At time $t = 466$ ps, the density of unbound pairs becomes small as compared to the exciton density, and the gain curves follow the decay of the A^{1S} excitonic population.

The temperature kinetics can be obtained from analysis of the width of the gain line. Taking into account the multiple reflections within the platelet as above, we obtain from (3)

$$\frac{S_{\alpha_M/2}}{S_{\alpha_M}} = e^{-\alpha_M d/2} \frac{1 - R^2 e^{2\alpha_M d}}{1 - R^2 e^{\alpha_M d}} , \qquad (9)$$

which yields the signal level corresponding to $\alpha_M/2$. Thus we obtain the width at half maximum of the gain line, $\Delta(h\nu)$, which in turn is related to the exciton tem-
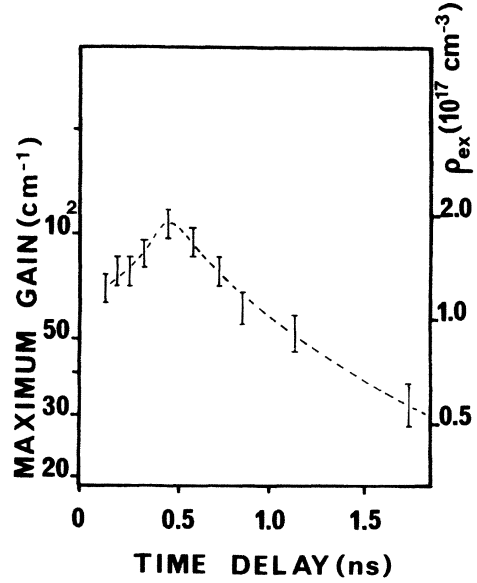

FIG. 5. Time behavior of the maximum gain of the A-LO process. Right vertical scale: exciton density kinetics taking $C_{eff} = 240$ cm^{-1}meV$^{-3/2}$. (The dashed line is a guide to the eye; vertical bars indicate uncertainty of α_M; for the uncertainty of ρ_{ex}, see the text—Sec. V.)

perature by

$$2.95 \ kT_{ex} \simeq \Delta(h\nu) . \qquad (10)$$

In fact, Eq. (10) is accurate as long as T_{ex} is larger than 10 K.[26] The exciton temperature kinetics are displayed in Fig. 6. At the beginning, T_{ex} is nearly constant and about $T_{ex} \simeq 20$ K ($133 < t \leq 266$ ps). Then, it decreases mono-
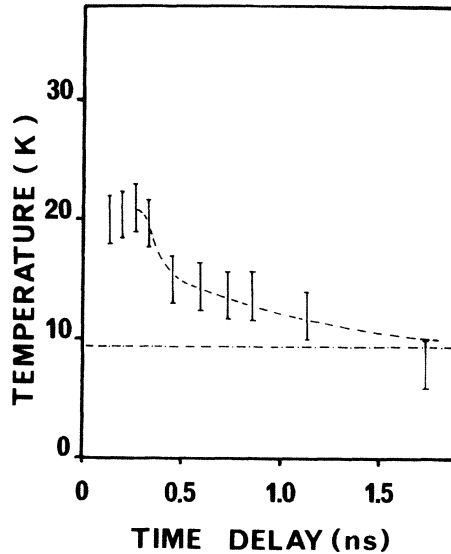

FIG. 6. Exciton temperature kinetics. The dashed-dotted line corresponds to the lattice temperature during the exciton kinetics (see text). (The dashed line is a guide to the eye; vertical bars indicate uncertainty.)

tonically down to the stable value of $T_{ex} \simeq 8$ K for delays $t \geq 1.7$ ns. This behavior is very similar to the one observed in previous time-resolved luminescence experiments, and can be explained on the ground of acoustical phonon emission by the excitonic gas.[17,19]

Under two-photon excitation, it is possible to estimate the initially created electron-hole pair density ρ_{init} as well as the final lattice temperature T_L independently from the previous method.[17,19] Starting from the measurement of the incident peak power on the platelet, ρ_{init} is given by the expression

$$\rho_{init} \simeq \frac{\beta \phi_{ex}^2 (1-R)^2 \Delta t}{2h\nu_{ex}[1+\beta\phi_{ex}(1-R)d]} , \tag{11}$$

with β as the two-photon absorption coefficient and Δt representing the pulse duration.

Using the data, $\beta = 0.03$cm/MW, $\Delta t \simeq 30$ ps, and $200 \leq \phi_{ex} \leq 300$ MW/cm^2 (which takes into account all the uncertainties of the experiment), we obtain

$$0.6 \times 10^{17} \leq \rho_{init} \leq 1.3 \times 10^{17} \text{ cm}^{-3} ,$$

which is somewhat lower than the maximum excitonic density deduced in Fig. 5:

$$1.4 \times 10^{17} \leq \rho_{max} \leq 3 \times 10^{17} \text{ cm}^{-3} .$$

This discrepancy may be attributed to the uncertainty in the determination of the effective coefficient C_{eff}. The final lattice temperature can be also determined from Ref. 17, on the ground of specific heat considerations:

$$T_L = \left[\frac{10}{\pi^2} (2h\nu - E_G) \frac{(\hbar\nu)^3}{k^4} \rho_{init} + T_b^4 \right]^{1/4} , \tag{12}$$

where ν is the mean sound velocity in the crystal.

This value is reached as soon as most of the initial kinetic energy of the created electron-hole pairs is transferred to the lattice, which is achieved for $t \geq 100$ ps.[32] We find, taking for the initial kinetic energy of the created electron-hole pairs the value $2h\nu - E_G \simeq 0.49$ eV:

$$8 < T_L < 9.5 \text{ K} ,$$

in good agreement with the exciton final temperature $(t > 1.7$ ns) shown in Fig. 6.

V. DISCUSSION OF SCREENING AT HIGH DENSITY

Let us examine the situation at short delay $(t \leq 133$ ps). The corresponding plasma density is $\rho = (2 \pm 1) \times 10^{17}$cm^{-3} estimated from two-photon pumping and lineshape analysis. We also know, from Fig. 3, that the exciton states are not stable for time ranging from 66 to 133 ps, since the corresponding resonances have disappeared from the transmission spectra. Therefore, the plasma density is higher than the Mott density.

Then, for time delays, in the range $133 \leq t \leq 200$ ps, the $1S$ exciton states can form (Figs. 3 and 4). The only way to account for this fact is to assume that the plasma density relaxes; this assumption is very reasonable, at least because we observe clearly stimulated emission on the EHP-LO process (see Fig. 4 at $t \simeq 66$ ps). As a conse-

quence, the screening efficiency of the Coulomb interaction in the plasma lowers, thus allowing the formation of bound electron-hole pairs. The estimated exciton density and temperature at $t \simeq 200$ ps are, respectively, $\rho_{ex} = (1.5 \pm 0.5) \times 10^{17}$ cm^{-3} and $T_{ex} = 20 \pm 2$ K. So the plasma density is now lower than or of the order of the Mott density. As the exciton density still increases at least by a factor ~ 1.33 between 200 and 466 ps (Fig. 5), the plasma density at $t \simeq 200$ ps can be estimated to be $\rho = (5 \pm 1.6) \times 10^{16}$ cm^{-3} (analyzing the LO-assisted excitonic line shape, which is the dominating process as soon as $t \geq 200$ ps, would lead to a slightly higher determination for ρ).

The understanding of transmissions experiments around the Mott transition is a complex task, since an accurate theory of the band-edge absorption for intermediate density regimes is necessary, including many-body effects such as band-gap renormalization, excitonic enhancement, and collision broadening.[33] As a starting point, we now compare our experimental data with the theoretical criterion (for determining the upper plasma density consistent with the electron-hole binding into exciton states) calculated in the frame of the static plasma screening theory;[34] the critical densities deduced from Ref. 34 are denoted hereafter ρ_M^S. On the reasonable assumption that, for $133 \leq t \leq 200$ ps, the plasma and the exciton temperatures are identical; we find $1.4 \times 10^{16} \leq \rho_M^S \leq 1.8 \times 10^{16}$cm^{-3}. The comparison of ρ_M^S with the plasma density determined experimentally just above, at $t \simeq 200$ ps indicates that the usual static Mott criterion underestimates the Mott density by a factor of about 3. A discrepancy of the same order can be deduced from the comparison between the dynamical screening calculation[33] and the static Mott criterion applied to cadmium sulfide.[35]

We turn now to the situation at long delay $(t > 1$ ns). We have determined from the experiments the kinetics of the exciton gas density and temperature (Figs. 5 and 6). We can deduce the unbound pair density by assuming that all the quasiparticules are in thermodynamical equilibrium at the same temperature, which is very reasonable for delays longer than, say, 200 ps. Using the mass action law between free carrier and excitons in the $1S$ state $(g_{ex} = 4)$, we deduce

$$\rho^2 = \frac{4}{g_{ex}} \rho_{ex} \left[\frac{m_c m_v kT}{M_{ex} 2\pi\hbar^2} \right]^{3/2} \exp \left[-\frac{E_B(t)}{kT} \right] . \tag{13}$$

Here, T is the temperature of the exciton-plasma system; ρ is the unbound electron-hole pair density; $m_{c(v)}$ is the conduction- (valence-) band effective mass; $E_B(t)$ is the exciton binding energy at time t, which satisfies $E_B(t) \leq E_{B0}$; and E_{B0} denotes the exciton binding energy at low density.

We use the material parameters: $m_c \simeq 0.13$, $m_v \simeq 0.8$, and $E_{B0} \simeq 16$ meV. For instance, at time $t = 1133$ ps, taking $T \simeq 12$ K, $\rho_{ex} = (9 \pm 3) \times 10^{16}$ cm^{-3}, and $E_B \simeq \frac{3}{4} E_{B0}$—since the $2S$ state begins to recover—we obtain $\rho \simeq 8 \times 10^{13}$ cm^{-3} (taking $E_B = E_{B0}$ would yield an even lower estimate for the plasma density). Two remarks are in order when analyzing the results at this delay.

(1) We know from the experiment that excitons are al-

most unscreened at this delay (Fig. 3). The plasma density becomes extremely low [$\rho \simeq 8 \times 10^{13}$ cm^{-3}, which is typically two orders of magnitude below the Mott density for $T = 12$ K, which is estimated from Ref. 33 at $\rho_M^S(T = 12$ K$) = 10^{16}$ cm^{-3}] so that free-carrier screening is expected to be insignificant.

(2) In the same time, Fig. 3 demonstrates that exciton screening is also very weak, even if the exciton density is about one order of magnitude higher than the static Mott density [$\rho_{ex} = (9 \pm 3) \times 10^{16}$ cm^{-3}]. We must stress that at the corresponding temperature $T = 12$ K, the same plasma density (even in dynamical calculation) is expected to strongly screen the exciton states, as is the case for time delays around 200 ps. We thus conclude that exciton screening is weak, as compared to free-carrier screening.

The analysis of the transient behavior of the $2S$ structure in the transmitted spectra gives additional information. Bound states of $2S$ type are present at time $t = 1733$ ps (see Fig. 3). The exciton density is then

$$\rho_{ex} = (5.5 \pm 2.5) \times 10^{16} \text{ cm}^{-3},$$

and the temperature $T_{ex} = 8 \pm 2$ K. Now the e-h unbound pairs have nearly disappeared from the system [as can easily be checked from (13)] so that the (e-h) system is now in a dense excitonic phase. The critical density estimated by

$$\rho_c(n = 2) = \frac{3}{4\pi} [a_B(n = 2)]^{-3},$$

[with $a_B(n = 2) = 4a_B(n = 1)$] yields here a correct estimate for the upper exciton density consistent with the $2S$ state appearance: taking $a_B(n = 1) \simeq 51$ Å, we obtain $\rho_c(n = 2) \simeq 3 \times 10^{16}$ cm^{-3} in agreement with the experimental value. This means that the $2S$ states become stable in a dense excitonic system when the mean volume per $1S$ exciton is greater than or of the order of the $2S$ exciton volume.

VI. CONCLUSION

We have investigated the electron-hole system in CdSe under strong picosecond excitation in the vicinity of the Mott density. The main original characteristics of this experiment are the following.

(1) We use two-photon absorption to generate a homogeneous plasma in the sample, which is extremely important in high excitation phenomena.

(2) We study by gain-absorption technique (time resolution 30 ps) both the spectral region of the direct processes (to get information on the bound states stability) and the region of the LO-phonon-assisted processes (to get information on the quasiparticle temperature and density).

From the analysis of our results, we deduce the exciton temperature kinetics and especially the kinetics of the exciton density. It must be stressed that the exciton density cannot be determined from luminescence techniques alone[17,19,21] so that this work represents, to our knowledge, the first study of the kinetics of this parameter.

We show that the A^{1S} exciton gas remains stable at densities about three times higher than expected from the static plasma screening theory. Concerning the $2S$ state, we conclude that it remains stable in an exciton gas up to densities around

$$\rho_c(n = 2) \simeq (3/4\pi)[4a_B(n = 1)]^{-3}.$$

All these experimental facts support the assertion that exciton screening is much weaker than plasma screening at the same temperature and density.

*Permanent address: A. F. Ioffe Physico-Technical Institute, Leningrad, 194021, U.S.S.R.

[1]C. Klingshirn and H. Haug, Phys. Rep. 70, 317 (1981).

[2]J. Shah, R. F. Leheny, and W. Wiegmann, Phys. Rev. B 16, 1577 (1976).

[3]V. G. Lyssenko, V. I. Revenko, F. G. Tartas, and V. G. Timofeev, Zh. Eksp. Teor. Fiz. 68, 335 (1975) [Sov. Phys.—JETP 41, 163 (1975)].

[4]F. Henneberger, J. Puls, H. Rossmann, and I. N. Uraltsev, Phys. Status Solidi B 121, K191 (1984).

[5]K. Bohnert, G. Schmieder, and C. Klingshirn, Phys. Status Solidi B 98, 175 (1980).

[6]J. Heidmann and T. Skettrup, Solid State Commun. 23, 27 (1977).

[7]C. Benoit a la Guillaume, J. M. Debever, and F. Salvan, Phys. Rev. 177, 567 (1969).

[8]K. L. Shacklee and R. F. Leheny, Appl. Phys. Lett. 18, 475 (1971).

[9]D. Magde and H. Mahr, Phys. Rev. Lett. 24, 890 (1970).

[10]E. Ostertag, R. Levy, and J. B. Grun, Phys. Status Solidi B 69, 629 (1975).

[11]J. M. Hvam, Solid State Commun. 26, 373 (1978).

[12]J. M. Hvam, Solid State Commun. 26, 987 (1978).

[13]D. Hulin, A. Antonetti, L. L. Chase, J. L. Martin, A. Migus, A. Mysyrowicz, J. P. Lowenau, S. Schmitt-Rink, and H. Haug, Phys. Rev. Lett. 52, 779 (1984).

[14]J. G. Fujitomo, S. G. Shevel, and E. P. Ippen, Solid State Commun. 49, 605(1984).

[15]G. W. Fehrenbach, W. Schafer, J. Treusch, and R. G. Ulbrich, Phys. Rev. Lett. 49, 128 (1982).

[16]M. Pugnet, A. Cornet, J. Collet, M. Brousseau, B. S. Razbirin, and G. V. Michailov, Solid State Commun. 36, 85 (1980).

[17]J. Collet, M. Pugnet, A. Cornet, M. Brousseau, B. S. Razbirin, and G. V. Michailov, Phys. Status Solidi B 103, 367 (1981).

[18]T. P. Daly and H. Mahr, Phys. Rev. B 29, 559 (1984).

[19]T. Amand, A. Cornet, M. Pugnet, J. Collet, M. Brousseau, and B. S. Razbirin. Phys. Status Solidi B 118, 113 (1983).

[20]A. Cornet, J. Collet, T. Amand, M. Pugnet, B. S. Razbirin,

and G. Michailov, J. Phys. Chem. Solids **44**, 53 (1983).

[21]T. Kobayachi, Y. Segawa, and S. Namba, Solid State Commun. **31**, 253 (1979).

[22]J. Collet and T. Amand, Phys. Rev. B **33**, 4129 (1986).

[23]For excitation induced spectra, the possible disturbing luminescence signal is subtracted. The latter is always much smaller than the probe signal in the analyzed time range.

[24]A. Kreissl, K. Bohnert, V. G. Lyssenko, and C. Klingshirn, Phys. Status Solidi B **114**, 537 (1982).

[25]R. Zimmermann, K. Kilimann, W. D. Kraeft, D. Kremp, and G. Ropke, Phys. Status Solidi B **90**, 175 (1978).

[26]V. A. Abramov, S. A. Permogorov, B. S. Razbirin, and A. I. Ekimov, Phys. Status Solidi **42**, 627 (1970).

[27]B. Segall and G. D. Mahan, Phys. Rev. **171**, 935 (1968).

[28]C. Hermann and P. Y. Yu, Solid State Commun. **28**, 313 (1978).

[29]Yu P. Gnatenko and M. V. Kurik, Opt. Spektrosk. **29**, 339 (1970) [Opt. Spectrosc. (USSR) **29**, 179 (1970)].

[30]D. G. Thomas, J. J. Hopfield, and M. Power, Phys. Rev. **119**, 570 (1960).

[31]R. B. Parsons, W. Wardzinski, and A. D. Yoffe, Proc. R. Soc. London, Ser. A **262** 120 (1961). In Ref. 30, the authors have shown that in CdS, for $20 \lesssim T_L \lesssim 86$ K, the absorption edge in the spectral region $E_{ex} - \hbar\omega_{LO} < h\nu < E_{ex}$ can be interpreted as the indirect process: photon + phonon LO$\rightarrow A$ exciton.

Expression (4) results from a second-order perturbation theory, in the case of light polarized perpendicular to the c axis. Applying this description to CdSe, we deduce from experimental results (Ref. 29): $200 \leq C_\perp \leq 445$ cm^{-1} meV$^{-3/2}$. For light polarized parallel to the c axis, in the spectral region of A-LO line, the absorption tail is weaker since the A intermediate state is forbidden, in the dipole approximation, by selection rules. Thus the A-LO process is described by indirect transitions involving virtual excited exciton states $(n > 1)$ and $B(n = 1)$ exciton states. In that case, we will still use (4) as a phenomenological expression and from the experimental results reported by R. B. Parsons *et al.*, we deduce that $C_\| \simeq 0.5 C_\perp$ in the short energy range around $E_{ex} - \hbar\omega_{LO}$. For our intermediate experimental configuration, we define an effective coefficient C_{eff} which satisfies $C_\| < C_{eff} < C_\perp$ and we take the central value $C_{eff} = (C_\| + C_\perp)/2$.

[32]J. Collet, A. Cornet, M. Pugnet, and T. Amand, Solid State Commun. **42**, 883 (1982).

[33]S. Schmitt-Rink, J. Lowenau, and H. Haug, Z. Phys. B **47**, 13 (1982).

[34]F. J. Rogers, H. C. Graboske, and D. J. Harwood, Phys. Rev. A **1**, 1577 (1970).

[35]For a plasma at $T = 60$ K in CdS, we deduce from Ref. 33 that the static Mott criterion underestimates the Mott density at least by a factor 3.